Title

Structural Insights into the Stability and Recognition Mechanism of the Antiquinalphos Nanobody for the Detection of Quinalphos in Foods

Journal

Analytical Chemistry, 95(30)

ISSN

0003-2700

Authors

Li, Jia-Dong

Wu, Guang-Pei

Li, Li-Hua

et al.

Publication Date

2023-08-01

DOI

10.1021/acs.analchem.3c01370

Peer reviewed

HHS Public Access

Author manuscript

Anal Chem. Author manuscript; available in PMC 2024 August 01.

Published in final edited form as:

Anal Chem. 2023 August 01; 95(30): 11306–11315. doi:10.1021/acs.analchem.3c01370.

Structural Insights into the Stability and Recognition Mechanism of Anti-Quinalphos Nanobody for the Detection of Quinalphos in Foods

Jia-Dong Li[1], **Guang-Pei Wu**[1], **Li-Hua Li**[2], **Lan-Teng Wang**[3], **Yi-Fan Liang**[1], **Ru-Yu Fang**[1], **Qiu-Ling Zhang**[1], **Ling-Ling Xie**[1], **Xing Shen**[1], **Yu-Dong Shen**[1], **Zhen-Lin Xu**[1,*], **Hong Wang**[1], **Bruce D. Hammock**[4]

[1]Guangdong Provincial Key Laboratory of Food Quality and Safety, National-Local Joint Engineering Research Center for Processing and Safety Control of Livestock and Poultry Products, College of Food Science, South China Agricultural University, Guangzhou 510642, China

[2]Future Technology Institute, South China Normal University, 510631, China

[3]CAS Key Laboratory of Quantitative Engineering Biology, Shenzhen Institute of Synthetic Biology, Shenzhen Institute of Advanced Technology, Chinese Academy of Sciences, Shenzhen 518055, China

[4]Department of Entomology and Nematology, UCD Comprehensive Cancer Center, University of California-Davis, California 95616, United States

Abstract

Nanobodies (Nbs) have great potential in immunoassays due to their exceptional physicochemical properties. With the immortal nature of Nbs and the ability to manipulate their structures using protein engineering it will become increasingly valuable to understand what structural features of Nbs drive high stability, affinity and selectivity. Here, we employed an anti-quinalphos Nb as model to illustrate the structural basis of Nbs' distinctive physicochemical properties and the recognition mechanism. The results indicated that the Nb-11A-ligand complexes exhibit a "tunnel" binding mode formed by CDR1, CDR2, and FR3. The orientation and hydrophobicity of small ligands are the primary determinants of their diverse affinities to Nb-11A. In addition, the primary factors contributing to Nb-11A's limited stability at high temperatures and in organic solvents are the rearrangement of the hydrogen bonding network and the enlargement of the binding cavity. Importantly, Ala 97 and Ala 34 at the active cavity's bottom and Arg29 and Leu73 at its entrance play vital roles in hapten recognition, which were further confirmed by mutant Nb-F3. Thus, our findings contribute to a deeper understanding of the recognition and stability

*Corresponding author: Zhen-Lin Xu, jallent@163.com; Tel: 020-85283448; Fax: 020-85280270.

The authors declare no competing financial interest.

ASSOCIATED CONTENT

Supporting Information

Reagents, materials and apparatus; Ic-Elisa protocol; Table of the X-ray data collection and refinement, panning strategy for anti-quinalphos nanobodies and mutants, the sequence of primers for mutation library construction, sensitivity and specificity of the Nb-11A and Nb-F3; Figures describing the hallmark hydrophilic amino acids of Nb, the reported binding mode of different Nbs against small molecule haptens, the small molecule haptens binding to Nbs, the structure of hapten H_1 and coating antigen.

mechanisms of anti-hapten Nbs and shed new light on the rational design of novel haptens and directed evolution to produce high-performance antibodies.

Graphical Abstract

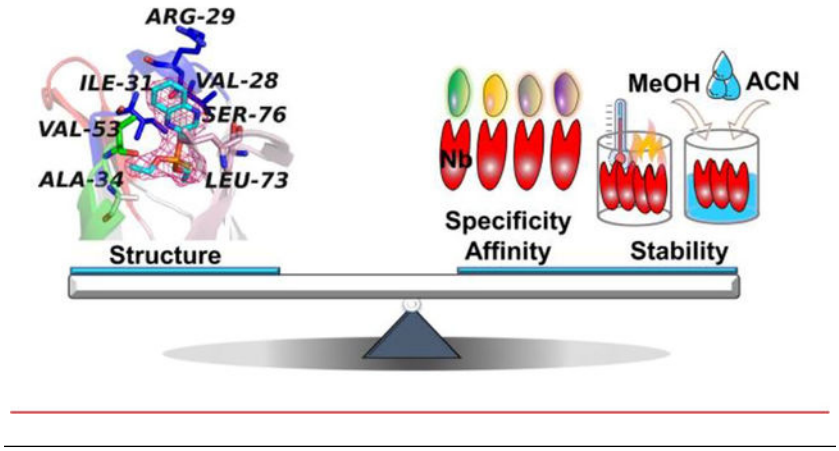

INTRODUCTION

As the primary element in an immunoassay, the recognition of the analyte by the antibody largely governs the performance of immunoassays. Therefore, there is an urgent need for the development of high-quality antibodies to enhance the sensitivity and specificity of immunoassays as well as to move toward antibodies of defined or immortal characteristics for consistency. The rapid progress of genetic engineering and protein engineering has led to the development of numerous approaches to antibody development, including conventional antibodies such as monoclonal antibody (mAb),[1] polyclonal antibody (pAb)[2] and genetically engineered antibodies like single chain fragments variable (scFv),[3–5] antigen binding fragments (Fab),[6, 7] and originally single-domain antibody or V_HH fragment commonly termed nanobody (Nb).[8, 9] It is important to note Nbs, which are a novel class of antibodies first discovered in 1993 by Hamers Casterman et al.,[10] generally produced from the variable domain of the heavy chain antibody in camels, llamas, alpacas and sharks, have been the subject of intense study in immunoassays due to their exceptional physicochemical properties, including tiny size, great solubility, and high stability.[11–15] Of course possibly the greatest attribute is that the nanobodies can be considered ‘immortal’ since they can be obtained through recombinant expression in a stable manner and can be easily modified *in vitro* through protein engineering.

As with other immunoassays, Nbs-based immunoassays are most easily generated for the detection of large molecules.[16–17] However, numerous assays for low-molecular weight compounds now have been reported, including insecticides,[18–19] toxins,[14, 20, 21] herbicides,[22, 23] and byproducts in food processing.[24] In spite of increasing research, there is limited structural information revealing the detailed mechanisms of hapten recognition with Nbs. Five hapten/Nbs complexes have so far been deposited in the protein data bank (PDB), two of them contain reactive red dye haptens,[25, 26] two of them involve

drug-related haptens,[27, 28] and one involves an antibacterial-antifungal compound.[29] The manner in which these haptens are bonded vary greatly and the structural mechanisms governing hapten-Nb interactions are still poorly understood. As a result, the majority of Nbs produced are still generated by "trial and error" or ease of hapten synthesis rather than a systematic design of immunizing haptens to gain the desired analyte recognition as has been done for poly and monoclonal antibodies.[30–31] With the immortal nature of nanobodies and the ability to manipulate their structures using protein engineering it will become increasingly valuable to understand what structural features of nanobodies drive high affinity and selectivity despite the lack of a V_L domain.

In this study, one of the most widely used organophosphate (OP) pesticides, quinalphos, was used as a model to prepare anti-quinalphos Nbs. After four successive rounds of panning, the resulting Nb (Nb-11A) exhibited good affinity to quinalphos. To gain understanding of the structural foundations of Nb-11A's recognition to ligands, the complex crystal structures of Nb-11A and quinalphos, and three analogues (parathion, triazophos, and coumaphos) were determined using X-ray crystallography. And then the key amino acids that form the binding pocket were identified by analyzing the interaction forces with ligands. Meanwhile, molecular dynamics (MD) was employed to study the Nb-11A's thermal stability and organic tolerance mechanism. Finally, the key role of the Ala 97 and Ala 34 at the active cavity's bottom and the Arg 29 and Leu 73 at its entrance for the recognition were further confirmed by a mutant Nb-F3 (Scheme 1). Through this study, the structural basis of Nbs' distinctive physicochemical properties as well as a better understanding of Nb-hapten interaction were gained, which will also facilitate the design of specific haptens and antibody affinity maturation *in vitro*.

EXPERIMENTAL SECTION

Reagents, materials and apparatus

The information about the used reagents, materials and apparatus can be found in the Supporting Information (Page S3).

Biopanning and characterization analysis of anti-quinalphos nanobodies

The phage display library was constructed by our lab previously[32] and four successive rounds of panning were performed as described before with some modifications (Table S1).[33] After four rounds of panning, 96 clones were analyzed by indirect competitive ELISA (ic-ELISA), and the positive clones were sequenced and transformed into *E. coli* BL21(DE3) and induced, followed by osmotic shock[34] and Ni-NTA purification procedures. After identification by SDS-PAGE and western blotting, the performance of the selected candidate Nb (Nb-11A) was characterized by ic-ELISA. The ic-ELISA was performed as described in the Supporting Information (Page S4). The thermostability and organic tolerance were also characterized (Supporting Information, Page S5).

Determination of affinity

All isothermal titration calorimetry (ITC) experiments were conducted with a MicroCal™ ITC_{200} (GE Healthcare, USA) as described before with minor modifications.[35] ITC trials

involved a total of 20 injections (2 μL) with a stirring speed of 1000 rpm. There should be a 150-second interval between injections, a 5-second noise filter time constant, and a high feedback mode. Origin and the manufacturer-supplied ITC add-on were used to examine the data.

Crystallization and data collection

Crystals of Nb-11A complexed with the pesticides (quinalphos, parathion, triazophos and coumaphos) were obtained using the sitting-drop method at 20°C. The purified Nb-11A (30 mg/mL) was mixed with pesticides at a molar ratio of 1:2. Drops consisting of 1 μL of the complex were mixed with 1 μL of 0.1 M citric acid pH 4.0, 5% (w/v) PEG 6000 (for Nb-11A/quinalphos), or 1 μL 0.1 M citric acid pH 3.5, 0.8 M ammonium sulfate (for Nb-11A/parathion, Nb-11A/triazophos and Nb-11A/coumaphos), respectively. Before being flash-cooled in liquid nitrogen, crystals were cryoprotected in a reservoir solution containing 30% glycerol. X-ray diffraction data were collected at 100 K on beamline BL02U1 and BL19U1 of the SSRF.

Determination and refinement of holo Nb-11A structure

Diffraction images were indexed and processed by XDS[36] and Dials.[37] The structure of holo Nb-11A was obtained by molecular replacement using PHASER MR from the CCP4 crystallography package[38] with PDB accession number 4WEN as the search model. The structure was refined using REFMAC,[39] PHENIX,[40] and COOT.[41] The structural parameters was shown in Table S2. All associated drawings were created with PyMOL.

Site-directed saturation mutation and characterization of mutants

Four key amino acid sites (Arg 29, Ala 34, Leu 73, and Ala 97) were introduced into Nb-11A using overlap extension PCR with the primers in Table S3. The biopanning procedures (Table S4) were executed with a modified solid phase coating in the microplate as described above. After three rounds of panning, 96 clones were chosen at random and induced on a 96-well deep-well plate. Positive plasmids obtained were transformed into *E. coli* BL21(DE3) and induced. After identification by SDS-PAGE, ic-ELISA was used to characterize the performance of the selected candidate mutants.

RESULTS AND DISCUSSION

Isolation and Identification of Anti-Quinalphos Nanobodies

A 1.43×10^7 *cfu*/mL library[32] was used for biopanning of anti-quinalphos Nbs according to the procedure shown in Table S1. After four rounds of panning, nine clones with inhibition rates for quinalphos (1 μg/mL) ranging from 45±0.31% to 83±0.14% were obtained (Figure 1A). Nb-11A with an inhibition rate of 80±0.18% and the highest potency was chosen for further analysis. As demonstrated by SDS-PAGE and western blotting (Figure 1B), the molecular weight of Nb-11A was about 17 kDa, and its purity was higher than 90% as determined by ImageJ.[42] The yield of Nb-11A was 15.0±0.5 mg/L. The hallmark hydrophilic amino acids ((F/Y) ER (A/R/G)) in FR 2 that differentiate many Nbs from conventional V_H (VGLW) are often thought to be the cause of Nbs' high solubility.[43] However, these four sites in Nb-11A were replaced by three hydrophobic amino acids

(37Y, 45P, and 47F) and a hydrophilic 44E (Figure S1), which caused the low solubility of Nb-11A.

The Binding Characteristics of Holo Nb-11A

The half maximal inhibitory concentration (IC_{50}) value for quinalphos was 298.3±1.2 ng/mL with the limit of detection (LOD) of 25.0±0.3 ng/mL (Figure 1C). Additionally, 9 kinds of quinalphos analogues were used for specificity analysis by cross-reactivity (CR) assay. As shown in Table S5, the IC_{50} of the assay for parathion, triazophos, and coumaphos were 554.9±1.6, 72.7±2.1, and 890.6±2.6 ng/mL, respectively, with a corresponding CR of 53±0.75%, 431±0.57%, and 41±0.46%. In addition, ITC data for the Nb-11A/pesticides (Figure 1, D to G) indicated that the K_D values were in good agreement with the ic-ELISA results. The K_D for Nb-11A binding to quinalphos, parathion, and triazophos were 14.3±0.4 nM, 16.7±0.7 nM, and 11.1±0.5 nM, respectively, which were all in the same level and 10-fold lower than the K_D for Nb-11A binding to coumaphos (174.0±1.3 nM).

Binding Mode

Although many Nbs against small molecule haptens have been reported, only several structures of Nbs and small molecule haptens have been elucidated. The binding patterns of these haptens are notably distinct.[25–29] To study the structural basis of pesticide recognition and its relationship to the reported binding capabilities, we determined the crystal structure of the Nb-11A/quinalphos, Nb-11A/parathion, Nb-11A/triazophos, and Nb-11A/coumaphos complex at 2.40 Å, 1.87 Å, 1.99 Å and 2.00 Å resolutions, respectively (Table S2). Instead of using the long CDR3 loop and the CDR2 interface surface to form a “lateral” binding mode,[25, 26] quinalphos, parathion, triazophos and coumaphos were inserted into the “tunnel” formed mainly by the CDR1, CDR2 and FR3 loop (Figure 2), which was comparable to the “tunnel” binding method of cortisol (Figure S2).[28] Interestingly, methotrexate (MTX) and triclocarban (TCC) were deeply entrenched in a distinct “tunnel” created by CDR1, CDR3, and FR1 loops (Figure S2).[27, 29] Previous Nb-antigen structures revealed that the binding affinity was mostly driven by the flexible CDR3 contact with the antigen, whereas CDR1 and CDR2 contributed only slightly to the interaction force.[44] Here, a comparison of these structures in “tunnel” binding mode reveals that the CDR1 is the major driven force in the “tunnel” architecture, which emphasizes the importance of CDR1 in recognition of these small ligands. Meanwhile, for “lateral” binding ligands, CDR1 also contributes some extra interaction force. All of these suggests that CDR1, rather than CDR3, plays an essential role in the recognition of at least these small ligands. Furthermore, the FR1 and FR3 play critical roles in the “tunnel” architecture, meaning that conserved FR is important as well. Cortisol (MW 362.5 Da),[28] MTX (MW 454.4 Da),[27] TCC (MW 315.6 Da),[29] and the ligands in this work (MW vary from 291.26 Da to 362.8 Da), which bound in a “tunnel” mode, are smaller than “lateral” binding reactive red 1 (MW 612)[26] and reactive red 6 (MW 628 Da)[25]. In addition, the molecules that bind in “tunnel” mode are lengthy and highly hydrophobic (Figure S2 and S3). Thus, size, shape, and solubility of small ligands appear to be the factors most likely to influence the binding mode of Nbs. Smaller molecules are more likely to bind in a “tunnel” mode, which can aid in the prediction of Nbs-small ligand recognition.

Specificity

All ligand atoms were visible and well-located in the electron density maps, with quinalphos, parathion, triazophos, and coumaphos deeply immersed in a “tunnel” formed by CDR1, CDR2, and FR3 loop in nearly the same orientation (Figure 3, A to D). In actuality, this hapten H_1 was initially made in order to generate antibodies with broad specificity for *O, O*-diethyl organophosphorus pesticides.[31] Therefore, it is not unexpected that Nb-11A can recognize other *O, O*-diethyl organophosphorus insecticides in addition to quinalphos. As expected, the common *O, O*-diethyl thiophosphate group of the four ligands was inserted into the bottom of the pocket of Nb-11A due to the easy accessibility of this group during immunization being remote from the site of attachment to the carrier protein (Figure S4). The percentage of ligand surface buried by Nb-11A was calculated to be 68% (326.9 $Å^2$), 63% (295.6 $Å^2$), 64% (330.9 $Å^2$) and 66% (362.7 $Å^2$) for quinalphos, parathion, triazophos and coumaphos, indicating an excellent surface complementarity between the pesticide ligands and Nb-11A.

Pesticide ligands were present in the hydrophobic pocket of Nb-11A through the hydrophobic interactions between Val 28, Arg 29, Ile 31 and Ala 34 of CDR1; Ile 51 and Val 53 of CDR2; Ala 97 from CDR3. Furthermore, residues of the nonhypervariable loop (Leu 4 and Cys 22 from FR1, Asp 72, Leu 73, Ser 76 and Val 78 from FR3) also contributed importantly to the binding. There only one weak hydrogen bond between sulfur of *O, O*-diethyl thiophosphate group and oxygen of Asp 72 was found in Nb-11A/parathion, Nb-11A/triazophos and Nb-11A/coumaphos. According to a generally held belief, hydrophobic forces dominate protein-ligand association, whereas charge-charge interactions and hydrogen bonds essentially govern the reaction specificity.[45–47] Due to the predominance of hydrophobic interaction in the binding force, Nb-11A could recognize quinalphos and its analogues (parathion, triazophos, and coumaphos). Specificity is one of the important properties of antibodies, which determines the performance of immunoassays based on these antibodies. We may alter the specificity of Nb-11A by site-directed mutation to widen its applicability while avoiding the time-consuming and unpredictable immunization and screening procedure. The key amino acid sites in the recognition process can be mutated to reshape the active cavity of Nb-11A. And then computer simulations can be used to calculate whether the mutant can effectively recognize other structural analogs of quinalphos. After a theoretical feasibility assessment, experimental validation of the mutation can proceed.

Affinity Differences

Despite the similarity of the amino acids involved in the hydrophobic binding pocket (Figure 3, A to D), there is a tiny differential in binding between Nb-11A and the four pesticide ligands due to the various characteristics of the ligands, resulting in differing affinities. In details, Val 28 and Ile 31 from CDR1, Val 53 from CDR2 and Leu 73 from FR3 provide conserved hydrophobic residues around the binding pocket entrance and pack against the hydrophobic upper end substructure of ligands, specifically the benzene ring and pyrazine ring of quinalphos, the benzene ring of parathion, the triazole ring and benzene ring of triazophos, furan ring and benzene ring of coumaphos (Figure 3, A to D). The positively charged Arg 29 at the entrance of the hydrophobic pocket stabilizes the interaction between

Nb-11A and parathion by forming a salt bridge between the sidechain guanidyl and the parathion nitroso group (Figure 3B). Nevertheless, the interaction between Arg 29 and the hydrophobic upper end substructure of quinalphos, triazophos and coumaphos might be unfavorable (Figure 3, A, C and D). Meanwhile, the lengthy sidechain of Arg 29 may additionally hinder the entrance of ligands due to steric hindrance. There is a weak hydrogen bond between the sulfur of the *O, O*-diethyl thiophosphate group and the oxygen of Asp 72 in Nb-11A/parathion (Figure 3B), Nb-11A/triazophos (Figure 3C), and Nb-11A/coumaphos (Figure 3D), but not in Nb-11A/quinalphos due to the little deviation of Asp 72 (Figure 3A). The P=S group of the *O, O*-diethyl thiophosphate group from quinalphos, parathion, and triazophos is hydrophobic, and its hydrophobicity is stronger than that of coumaphos (Figure 3, E to H), resulting in stronger binding to Leu 73, which accounts for the much higher affinity of Nb-11A for quinalphos, parathion, and triazophos than for coumaphos.

Thermal Stability of Nb-11A

The results of a thermostability investigation (Figure 4, A and B) revealed that Nb-11A retained approximately 100% of its binding activity after 5 min at 80°C. Even at 95°C for 60 min, Nb-11A was able to retain over 40% of its binding activity. The excellent thermostability of Nb-11A is attributed to the special steric structure of Nbs.[11, 48–50] According to the structure of Nb-11A, Cys 22 in framework region (FR) 1 and Cys 95 in FR3 form a conserved disulfide bond (Figure 2A), which resulting in the robustness of Nb-11A to high temperature. However, compared to other Nbs,[30, 51–53] the thermal stability of Nb-11A is not outstanding. This may be because Nb-11A lacks the extra disulfide link between complementarity determining region (CDR) 1 and CDR3, which is thought to be necessary for strong thermostability due to its role in reducing paratope flexibility.[43, 48, 54] Given that the interloop disulfide bonds are more likely to be present in Nbs with longer CDR3 and the median value for CDR3 length of Nbs is 16 aa,[43, 55] the presence of an additional disulfide link between CDR1 and CDR3 (11 aa) of Nb-11A seems improbable.

Next, we conducted MD simulation at 310 K (37°C) and 368 K (95°C) to further assess the thermostability of the Nb-11A. The average root mean square deviation (RMSD) values of Nb-11A at 310 K (0.15±0.03 nm) were much lower than that at 368 K (0.33±0.07 nm) after a 20-ns molecular dynamic simulation (Figure 4C), which was consistent with Nb-11A's thermostability. The root mean square fluctuation (RMSF) values often reflect the fluctuation of individual residues during the MD simulation process. As shown in Figure 4D, the fluctuation of three loop regions (Res 52–57, Res 61–65, and Res 101–104) were higher at 368 K than at 310 K, suggesting that their flexibility increased with a rise in temperature. There was no apparent structural change of Nb-11A after 20-nm MD simulation at 310 K (Figure 4G). However, comparing the conformations of these three loop regions (Res 52–57, Res 61–65 and Res 101–104) at 368 K in MD equilibrium, the locations of these three loops shift by between 9.1 Å to 9.7 Å (Figure 4H), affecting the binding of Nb-11A and resulting in decreased stability. Importantly, Res 52–57 from CDR2 is the component of binding pocket and move almost 40 degrees out of the pocket, indicating that in addition to the FR as reported,[56] CDRs also play an important role for the thermostability of Nb. Additionally, the number of H-bonds between Nb-11A and water is 246 and 201, respectively, at 310 and 368 K, and there are 87 and 80 H-bonds in the structure of Nb-11A itself (Figure 4, E and

F). The stability of Nb-11A at 368 K is likewise negatively impacted by the decline in the number of systematic H-bonds.[57, 58]

Organic Solvent Tolerance of Nb-11A

In order to improve the extraction efficiency of chemical contaminants, organic reagents are frequently used in the pretreatment of samples. Here, MeOH and CAN were used to evaluate Nb-11A's organic tolerance. As the results showed (Figure 5A), Nb-11A displayed almost 100% binding activity in 10% MeOH and 10% ACN and nearly 50% binding activity in 30% MeOH and 25% ACN. Thus, Nb-11A shown a high tolerance to MeOH and ACN, corresponding with the results of anti-carbofuran Nb 316,[18] anti-parathion Nb VHH9,[32] and anti-iso-tenuazonic acid Nb B3G3.[59] The superior organic solvent tolerance may result in a simple pre-treatment process for the detection of practical samples.

To evaluate the Nb-11A's resistance to organic solvents in further detail, we conducted MD simulation in 10% MeOH, 10% ACN, 80% MeOH and 40% ACN respectively, for Nb-11A remained intact binding activity in 10% MeOH and 10% ACN, and lost its binding activity in 80% MeOH and 40% ACN. As shown in Figure 5, B and C, the system achieved equilibrium after 20 ns of simulation. The total number of the H-bonds between Nb-11A and the solvent during the simulation were shown in Figure 5, D to G, the total H-bonds number of Nb-11A in 10% MeOH and 80% MeOH system was about 312 and 290 respectively, while that of 10% ACN and 40% ACN was only 273 and 235, respectively. The stability of Nb-11A is reduced as a result of the network of H-bonds being rearranged.[57, 58] In addition, there were three regions (Res 25–29, Res 52–57 and Res 71–76) located on binding pocket whose fluctuation were higher in 80% MeOH than in water (Figure 5H) attributed to the conversion from the alpha helix to the loop structure while in the presence of the MeOH solvent (Figure 5K). Meanwhile, the same three fluctuation regions also existed in 40% ACN (Figure 5, I to M). However, there was no discernible difference between the fluctuation of the binding pocket in 10% MeOH and 10% ACN and that in water (Figure 5, H to L). According to a comparison of their conformations in MD equilibrium, these three regions (Res 25–29, Res 52–57 and Res 71–76) moved by between 4.7 Å-10.1 Å in 80% MeOH and 4.3 Å-7.9 Å in 40% ACN (Figure 5, K and M). Importantly, Res 52–57 moved out of the pocket by about 60 degrees and 30 degrees, respectively, in 80% MeOH and 40% ACN (Figure 5, K and M). The movement of these three regions enlarged the binding pocket from 444.0 $Å^3$ to 707.4 $Å^3$ (in 80% MeOH) and 626.6 $Å^3$ (in 40% ACN), which is the main reason for the inactivation of Nb-11A.

Site-Directed Saturation Mutation

In order to confirm the key role of four sites (Ala 97 and Ala 34 at the active cavity's bottom and the Arg29 and Leu73 at its entrance) in the atomic level mechanics of the molecular recognition that take place, we constructed a Arg 29, Ala 34, Leu 73 and Ala 97 saturated mutations library (Figure S5) and the Nb-F3 with inhibition levels of quinalphos (1 μg/mL) of more than 90% was selected from the secondary saturation mutation library for further analysis (Figure S6 and S7). As shown in Figure 6A, the molecular weight of Nb-F3 was approximately 17 kDa, which is comparable with Nb-11A. The yield of Nb-F3 was 1.0±0.2 mg/L. According to the results of sequence alignment (Figure 6D), Nb-F3 differed

from parent Nb-11A by 3 sites, which may explain the variation in expression level, as these modifications render hydrophobic characteristics to Nb-F3.[43] As demonstrated by the standard curve in Figure 6B, Nb-F3 (IC_{50}=67.4±1.5 ng/mL, LOD=6.4±0.7 ng/mL) exhibited 4.4 fold higher sensitivity and 3.9 fold higher LOD than the parent Nb-11A (IC_{50}=298.3±1.2 ng/mL, LOD=25.0±0.3 ng/mL) for the detection of quinalphos. Leu 73 from FR3 of Nb-F3 stayed the same as Nb-11A (Figure 6D), and the likelihood of Leu 73 among the 15 positive sequences was 67%, indicating that Leu 73 may play a key role in the binding of ligands. As depicted in Figure 6C, Leu 73, which is highly hydrophobic, packed tightly against the hydrophobic rings of pesticide ligands surrounding the entrance of the pocket, stabilizing the pesticide ligands; this might have been the reason why Leu 73 is so critical. Arg 29 Asn positioned at the entrance of the pocket expanded the pocket entrance, which could be advantageous for the loading of ligands (Figure 6C). Meanwhile, the longer side chains of Ala 34 Cys and Ala 97 Val on the bottom of the pocket made the bottom of the pocket smaller (from 425.8 $Å^3$ to 344.3 $Å^3$), shallower (from 17.1 Å to 14.0 Å) and more hydrophobic (Figure 6C), hence tightening the binding of ligands to Nb-F3, which indicated that the adjustment of the active cavity size, especially the size of the entrance and the bottom, would be a worthwhile strategy to take into account for directed evolution to produce high-performance antibodies.

CONCLUSIONS

In summary, anti-quinalphos nanobody Nb-11A was isolated and exhibited an affinity range of 14.3±0.4 nM to 174.0±1.3 nM for quinalphos and three analogues (parathion, triazophos, and coumaphos). To elucidate the structural basis of Nb-11A' distinctive physicochemical properties as well as the recognition mechanism between Nb-11A and the four pesticide ligands, high-resolution crystal structures of the Nb-11A complex were solved.

1. As expected, the *O, O*-diethyl thiophosphate group of the ligands was inserted into the bottom of the "tunnel" formed by CDR1, CDR2, and FR3 loop in nearly the same orientation due to the easy accessibility of this group during immunization.
2. Due to the predominance of hydrophobic interaction in the major binding force, Nb-11A could recognize quinalphos and its analogues (parathion, triazophos, and coumaphos).
3. The difference in hydrophobicity of the *O, O*-diethyl thiophosphate group of the ligands is the determining factor in the binding affinity differences of Nb-11A to the four pesticide ligands.
4. Under conditions of high temperature (95°C), 80% MeOH, and 40% ACN, the network of H-bond was rearranged and the binding pocket was enlarged, affecting the binding to pesticides and reducing the stability of Nb-11A.

Ultimately, the vital role of Ala 97 and Ala 34 at the active cavity's bottom and the Arg 29 and Leu 73 at its entrance played in hapten recognition were further confirmed by a four site-directed saturation mutant Nb-F3, which exhibited a better performance in sensitivity and specificity. Thus, this work demonstrated that structure-guided evolution,

which employed targeted mutagenesis, is effective for maximizing the efficiency to obtain antibodies with better sensitivity or specificity. The sensitivity and specificity of Nb-F3 still have potential for further enhancement. Therefore, in the future, we can conduct a new round of evolution based on structural analysis to obtain superior antibodies. The key amino acid sites in the recognition process can be mutated to reshape the active cavity of Nb-11A. And then computer simulations can be used to calculate whether the mutant can effectively recognize quinalphos or other structural analogs. After a theoretical feasibility assessment, experimental validation of the mutation can proceed. On the other hand, a better understanding of the recognition of Nb-11A to quinalphos and its analogues could also facilitate rationalizing the design of specific haptens. The specificity of the hapten directly determines the specificity of the obtained antibody. Therefore, in order to obtain an antibody with good specificity to quinalphos, when designing the hapten, the carrier protein should be connected to the *O, O*-diethyl thiophosphate group as much as possible, or consideration should be given to removing the *O, O*-diethyl thiophosphate group, to maximize the exposure of benzene ring and pyrazine ring.

Supplementary Material

Refer to Web version on PubMed Central for supplementary material.

ACKNOWLEDGMENTS

This work was supported by the National Key R&D Program of China (2019YFE0116600), the Guangdong Provincial Science and Technology Project (2022A0505050061), the Natural Science Foundation of China (31972157) and the Guangdong Province Universities and Colleges Pearl River Scholar Funded Scheme (2017). Partial support was provided by NIH-NIEHS (RIVER Award) R35 ES030443–01 and NIH-NIEHS (Superfund Award) P42 ES004699.

Data availability

All data generated or analysed during this study are included in this published article (and its Supplementary Information files). The structural models generated in this study have been deposited in the Protein Data Bank under the accession codes 8H7I (Nb-11A/quinalphos), 8H7M (Nb-11A/parathion), 8H7N (Nb-11A/triazophos) and 8H7R (Nb-11A/coumaphos).

REFERENCES

1. Köhler G, Milstein C, Continuous cultures of fused cells secreting antibody of predefined specificity. nature 1975, 256(5517), 495–497. [PubMed: 1172191]
2. Overkamp D, Mohammed-Ali S, Cartledge C, et al. , Production of polyclonal antibodies in ascitic fluid of mice: technique and applications. J. Immunoassay 1988, 9(1), 51–68. [PubMed: 3283169]
3. Wang F, Li N, Zhang Y, et al. , Preparation and directed evolution of anti-ciprofloxacin ScFv for immunoassay in animal-derived food. Foods 2021, 10(8), 1993. [PubMed: 34574102]
4. Denizci Öncü M, Balcioğlu BK, Özgür B, et al. , Structure-based engineering of an antiangiogenic scFv antibody for soluble production in E. coli without loss of activity. Appl. Biochem. 2022, 69(5), 2122–2137.
5. Laroche Y, Demaeyer M, Stassen JM, et al. , Characterization of a recombinant single-chain molecule comprising the variable domains of a monoclonal antibody specific for human fibrin fragment D-dimer. J. Biol. Chem. 1991, 266(25), 16343–16349. [PubMed: 1885569]

6. Flanagan RJ, Jones AL, Fab antibody fragments: some applications in clinical toxicology. Drug Saf. 2004, 27(14), 1115–1133. [PubMed: 15554746]
7. Darwish M, Shatz W, Leonard B, et al. , Nanolipoprotein particles as a delivery platform for Fab based therapeutics. Bioconjugate Chem. 2020, 31(8), 1995–2007.
8. Salvador JP, Vilaplana L, Marco MP, Nanobody: outstanding features for diagnostic and therapeutic applications. Anal. Bioanal. Chem. 2019, 411(9), 1703–1713. [PubMed: 30734854]
9. Muyldermans S, Applications of Nanobodies. Annu. Rev. Anim. Biosci. 2021, 9, 401–421. [PubMed: 33233943]
10. Hamers-Casterman C, Atarhouch T, Muyldermans S, et al. , Naturally occurring antibodies devoid of light chains. Nature 1993, 363(6428), 446–448. [PubMed: 8502296]
11. Muyldermans S, Nanobodies: Natural single-domain antibodies. Annu. Rev. Biochem. 2013, 82, 775–797. [PubMed: 23495938]
12. Liu M, Li L, Jin D, et al. , Nanobody-A versatile tool for cancer diagnosis and therapeutics. Wiley Interdiscip. Rev.: Nanomed. Nanobiotechnol. 2021, 13(4), e1697. [PubMed: 33470555]
13. Pérez JM, Renisio JG, Prompers JJ, et al. , Thermal unfolding of a llama antibody fragment: a two-state reversible process. Biochemistry 2001, 40(1), 74–83. [PubMed: 11141058]
14. He T, Wang Y, Li P, et al. , Nanobody-based enzyme immunoassay for aflatoxin in agro-products with high tolerance to cosolvent methanol. Anal. Chem. 2014, 86(17), 8873–8880. [PubMed: 25079057]
15. Kim HJ, McCoy MR, Majkova Z, et al. , Isolation of alpaca anti-hapten heavy chain single domain antibodies for development of sensitive immunoassay. Anal. Chem. 2012, 84(2), 1165–1171. [PubMed: 22148739]
16. Su RF, Wu YT, Doulkeridou S, et al. , A nanobody-on-quantum dot displacement assay for rapid and sensitive quantification of the epidermal growth factor receptor (EGFR). Commun. 2022, 61(33), e202207797.
17. Bai MF, Wang YQ, Zhang C, et al. , Nanobody-based immunomagnetic separation platform for rapid isolation and detection of Salmonella enteritidis in food samples. Food Chem. 2023, 424, 136416. [PubMed: 37247600]
18. Zhang JR, Wang Y, Dong JX, et al. , Development of a simple pretreatment immunoassay based on an organic solvent-tolerant nanobody for the detection of carbofuran in vegetable and fruit samples. Biomolecules 2019, 9(10), 576. [PubMed: 31591300]
19. Luo L, Lin SQ, Wu ZY, et al. , Nanobody-based fluorescent immunoassay using carbon dots anchored cobalt oxyhydroxide composite for the sensitive detection of fenitrothion. J. Hazard. Mater. 2022, 439, 129701. [PubMed: 36104918]
20. Ren W, Li Z, Xu Y, et al. , One-step ultrasensitive bioluminescent enzyme immunoassay based on nanobody/nanoluciferase fusion for detection of aflatoxin B_1 in cereal. J. Agric. Food Chem. 2019, 67(18), 5221–5229. [PubMed: 30883117]
21. Wang X, Wang Y, Wang Y, et al. , Nanobody-alkaline phosphatase fusion-mediated phosphate-triggered fluorescence immunoassay for ochratoxin a detection. Spectrochim Acta A Mol Biomol Spectrosc 2020, 226, 117617. [PubMed: 31605970]
22. Zhang YY, Li LH, Wang Y, et al. , Ultrasensitive and rapid colorimetric detection of paraquat via a high specific VHH nanobody. Biosens Bioelectron 2022, 205, 114089. [PubMed: 35196601]
23. Li ZF, Dong JX, Vasylieva N, et al. , Highly specific nanobody against herbicide 2,4-dichlorophenoxyacetic acid for monitoring of its contamination in environmental water. Sci. Total Environ. 2021, 753, 141950. [PubMed: 32906044]
24. Liang YF, Zeng YY, Luo L, et al. , Detection of acrylamide in foodstuffs by nanobody-based immunoassays. J. Agric. Food Chem. 2022, 70(29), 9179–9186. [PubMed: 35819336]
25. Spinelli S, Frenken LGJ, Hermans P, et al. , Camelid heavy-chain variable domains provide efficient combining sites to haptens. Biochemistry 2000, 39(6), 1217–1222. [PubMed: 10684599]
26. Spinelli S, Tegoni M, Frenken L, et al. , Lateral recognition of a dye hapten by a llama VHH domain. J. Mol. Biol. 2001, 311(1), 123–129. [PubMed: 11469862]
27. Fanning SW, Horn JR, An anti-hapten camelid antibody reveals a cryptic binding site with significant energetic contributions from a nonhypervariable loop. Protein science: a publication of the Protein Society 2011, 20(7), 1196–1207. [PubMed: 21557375]

28. Ding L, Wang Z, Zhong P, et al. , Structural insights into the mechanism of single domain VHH antibody binding to cortisol. FEBS Lett 2019, 593(11), 1248–1256. [PubMed: 31049949]
29. Rosa ST, Wogulis LA, Wogulis MD, et al. , Structure and specificity of several triclocarban-binding single domain camelid antibody fragments. J. Mol. Recognit. 2019, 32(1), e2755. [PubMed: 30033524]
30. Goodrow MH, Harrison RO, and Hammock BD, Hapten Synthesis, antibody development, and competitive inhibit ion enzyme immunoassay for s-Triazine herbicides. J. Agric. Food Chem. 1990, 38(4), 990–996.
31. Xu ZL, Xie GM, Li YX, et al. , Production and characterization of a broad-specificity polyclonal antibody for *O, O*-diethyl organophosphorus pesticides and a quantitative structure-activity relationship study of antibody recognition. Anal. Chim. Acta. 2009, 647(1), 90–96. [PubMed: 19576391]
32. Zhang YQ, Xu ZL, Wang F, et al. , Isolation of bactrian camel single domain antibody for parathion and development of one-step dc-FEIA method using VHH-alkaline phosphatase fusion protein. Anal. Chem. 2018, 90(21), 12886–12892. [PubMed: 30256086]
33. Wang F, Li ZF, Yang YY, et al. , Chemiluminescent enzyme immunoassay and bioluminescent enzyme immunoassay for tenuazonic acid mycotoxin by exploitation of nanobody and nanobody-nanoluciferase fusion. Anal. Chem. 2020, 92(17), 11935–11942. [PubMed: 32702970]
34. Lorimer IA, Keppler-Hafkemeyer A, Beers RA, et al. , Recombinant immunotoxins specific for a mutant epidermal growth factor receptor: targeting with a single chain antibody variable domain isolated by phage display. Proc. Natl. Acad. Sci. U. S. A. 1996, 93(25), 14815–14820. [PubMed: 8962138]
35. Maso K, Montagner IM, Grigoletto A, et al. , A non-covalent antibody complex for the delivery of anti-cancer drugs. Eur. J. Pharm. Biopharm. 2019, 142, 49–60. [PubMed: 31201855]
36. Kabsch W, XDS. Acta Crystallogr., Sect. D: Biol. Crystallogr. 2010, 66(Pt 2), 125–132.
37. Winter G, Beilsten-Edmands J, Devenish N, et al. , DIALS as a toolkit. Protein Sci. 2022, 31(1), 232–250. [PubMed: 34747533]
38. Nonaka T, The CCP4 suite-computer programs for protein crystallography. X-RAYS 2010, 36(3), 224–227.
39. Vagin AA, Steiner RA, Lebedev AA, et al. , REFMAC5 dictionary: organization of prior chemical knowledge and guidelines for its use. Acta Crystallographica 2010, 60(Pt 12 Pt 1), 2184–2195.
40. Storoni LC, Terwilliger TC, Adams PD, et al. , Automated structure solution with the PHENIX suite. Methods Mol. Biol. 2008, 426, 419–435. [PubMed: 18542881]
41. Emsley P, Lohkamp B, Scott W, et al. , Features and development of Coot. Acta Crystallogr D Biol. Crystallogr. 2010, 66(Pt 4), 486–501. [PubMed: 20383002]
42. Alonso Villela SM, Kraïem H, Balkiss BZ, et al. , A protocol for recombinant protein quantification by densitometry. MicrobiologyOpen, 2020, 9(6), 1175–1182. [PubMed: 32255275]
43. Govaert J, Pellis M, Deschacht N, et al. , Dual beneficial effect of interloop disulfide bond for single domain antibody fragments. J. Biol. Chem. 2012, 287(3), 1970–1979. [PubMed: 22128183]
44. Mitchell LS, Colwell LJ, Comparative analysis of nanobody sequence and structure data. Proteins 2018, 86(7), 697–706. [PubMed: 29569425]
45. Arevalo JH, Stura EA, Taussig MJ, et al. , Three-dimensional structure of an anti-steroid Fab′ and progesterone-Fab′ complex. J. Mol.Bio. 1993, 231(1), 103–118. [PubMed: 8496956]
46. Webster DM, Henry AH, & Rees AR, Antibody-antigen interactions. Curr. Opin. Struct. Biol. 1994, 4(2), 123–129.
47. Trinh CH, Hemmington SD, Verhoeyen ME et al. , Antibody fragment Fv4155 bound to two closely related steroid hormones: the structural basis of fine specificity. Structure 1997, 5(7), 937–948. [PubMed: 9261086]
48. Kunz P, Flock T, Soler N, et al. , Exploiting sequence and stability information for directing nanobody stability engineering. Biochim. Biophys. Acta, Gen. Subj. 2017, 1861(9), 2196–2205. [PubMed: 28642127]
49. Kunz P, Zinner K, Mücke N, et al. , The structural basis of nanobody unfolding reversibility and thermoresistance. Sci. Rep. 2018, 8(1), 7934. [PubMed: 29784954]

50. Bond CJ, Marsters JC, Sidhu SS, Contributions of CDR3 to VHH domain stability and the design of monobody scaffolds for naive antibody libraries. J. Mol. Biol. 2003, 332(3), 643–655. [PubMed: 12963373]
51. Chen J, He QH, Xu Y, et al. , Nanobody medicated immunoassay for ultrasensitive detection of cancer biomarker alpha-fetoprotein. Talanta 2016, 147, 523–530. [PubMed: 26592642]
52. Liu X, Tang Z, Duan Z, et al. , Nanobody-based enzyme immunoassay for ochratoxin A in cereal with high resistance to matrix interference. Talanta 2017, 164, 154–158. [PubMed: 28107910]
53. Wang J, Bever CR, Majkova Z, et al. , Heterologous antigen selection of camelid heavy chain single domain antibodies against tetrabromobisphenol A. Anal. Chem. 2014, 86(16), 8296–8302. [PubMed: 25068372]
54. Genst ED, Handelberg F, Meirhaeghe AV, et al. , Chemical basis for the affinity maturation of a camel single domain antibody. J. Biol. Chem. 2004, 279(51), 53593–53601. [PubMed: 15383540]
55. Vattekatte AM, Shinada NK, Narwani TJ, et al. , Discrete analysis of camelid variable domains: sequences, structures, and in-silico structure prediction. PeerJ 2020, 8, e8408. [PubMed: 32185102]
56. Saerens D, Pellis M, Loris R, et al. , Identification of a universal VHH framework to graft non-canonical antigen-binding loops of camel single-domain antibodies. J. Mol. Biol. 2005, 352(3), 597–607. [PubMed: 16095608]
57. Sigala PA, Ruben EA, Liu CW, et al. , Determination of hydrogen bond structure in water versus aprotic environments to test the relationship between length and stability. J. Am. Chem. Soc. 2015, 137(17), 5730–5740. [PubMed: 25871450]
58. Pace CN, Scholtz JM, Grimsley GR, Forces stabilizing proteins. FEBS Lett 2014, 588(14), 2177–2184. [PubMed: 24846139]
59. Wang F, Yang YY, Wan DB, et al. , Nanobodies for accurate recognition of iso-tenuazonic acid and development of sensitive immunoassay for contaminant detection in foods. Food Control 2002, 136, 108835.

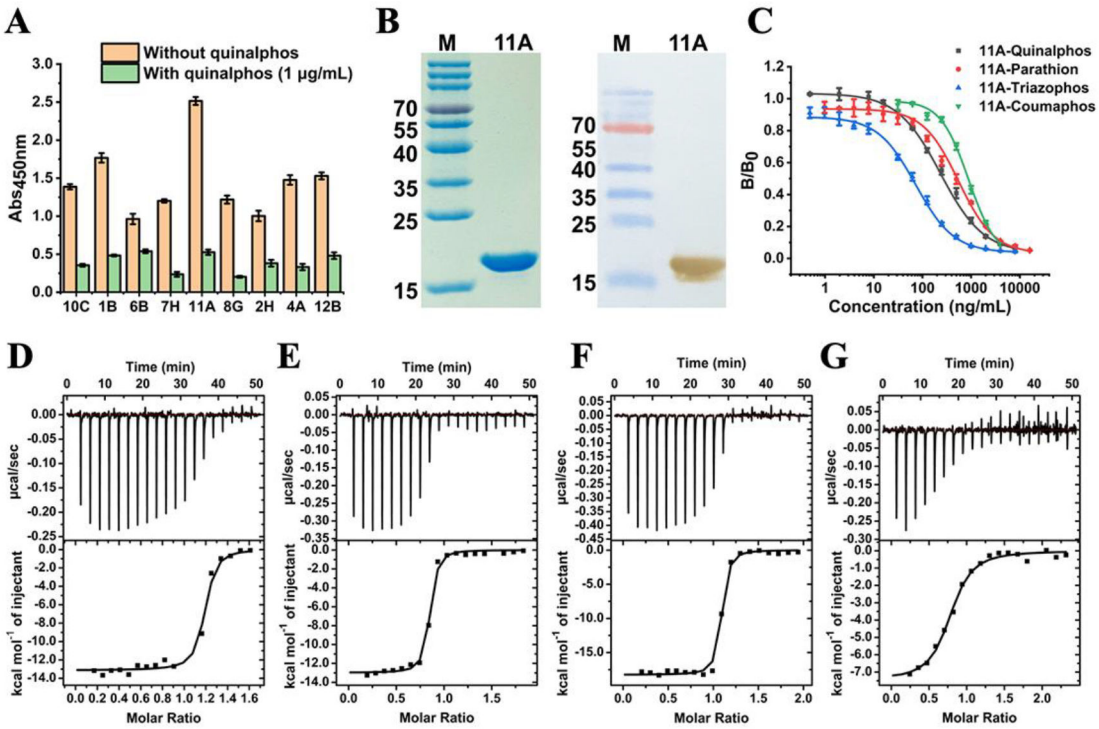

Figure 1. Preparation and identification of anti-quinalphos nanobodies.

(**A**) The sensitivity analysis of nine positive clones by ic-ELISA. The orange bars mean the potency and the green bars mean the inhibition in the presence of quinalphos (1 μg/mL). The inhibition rate= (potency value-inhibition value)/potency value×100%. (**B**) SDS-PAGE and western blotting analysis of purified Nb-11A. (**C**) The standard curve of ic-ELISA based on Nb-11A. (**D to G**) The binding isotherm and plotted titration curve for the binding of quinalphos (D), parathion (E), triazophos (F) and coumaphos (G) to Nb-11A at pH 7.4 and 25°C.

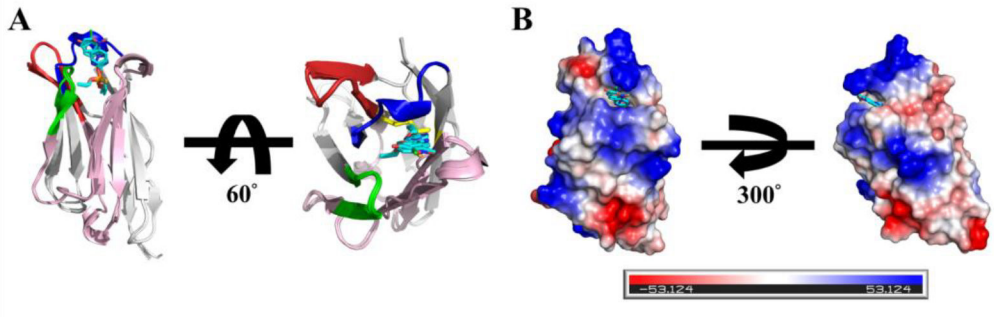

Figure 2. Overall structure of pesticides ligand bound to Nb-11A.

(**A**) An overlap of the holo Nb-11A structure shows the similarity between the structures. CDR1, CDR2, CDR3 and FR3 are shown in blue, green, tv-red and light pink, respectively. The disulphide bridge is indicated in yellow connecting two cysteines. (**B**) The electrostatic potential distribution at the molecular surfaces of holo Nb-11A (negative in red, positive in blue and neutral in white).

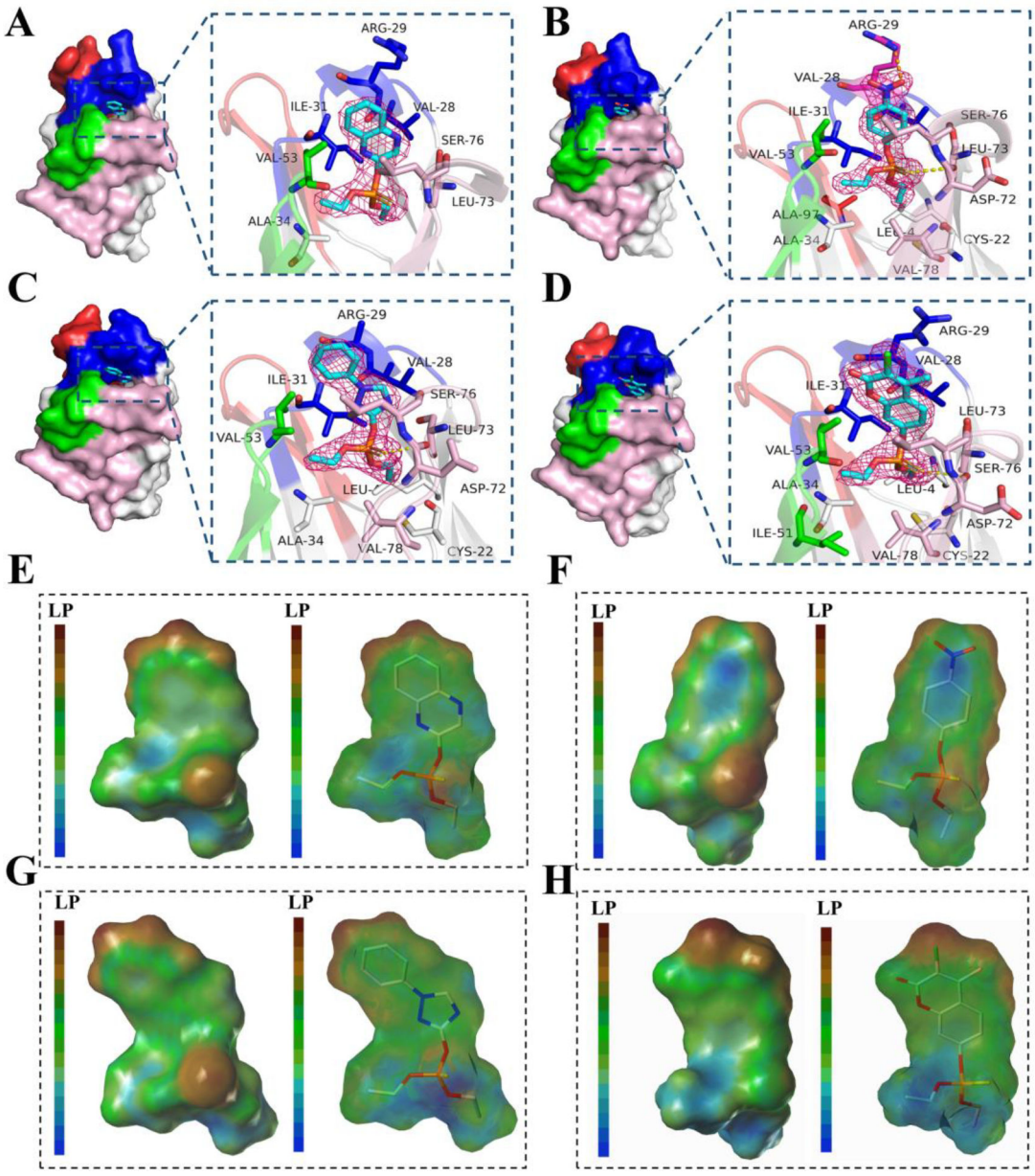

Figure 3. The binding poses of Nb-11A to pesticide ligands and the pesticide ligands' hydrophobic properties.

(**A to D**) Details of the interaction between Nb-11A and quinalphos (A), parathion (B), triazophos (C) and coumaphos (D). The unbiased 2Fo-Fc density corresponding to the ligands are contoured at 1σ. The carbon atom, nitrogen atom, oxygen atom, phosphorus atom, sulfur atom, chlorine atom of the ligands are shown in cyan, blue, tv_red, orange, yellow-orange and green, respectively. The side chains of Nb-11A directly interacting with the ligands are shown in sticks and labeled. CDR1, CDR2, CDR3 and FR3 are shown in blue, green, tv-red and light pink, respectively. (**E to H**) The lipophilic surface of quinalphos (E), parathion (F), triazophos (G) and coumaphos (H) in opaque (the left) and transparent (the right) presentation calculated by SYBYL (Provided by professor Xin'an Huang from

Guangzhou University of Chinese Medicine). The color ramp is the default condition and the closer the color is to the top of the color ramp, the more hydrophobic it is.

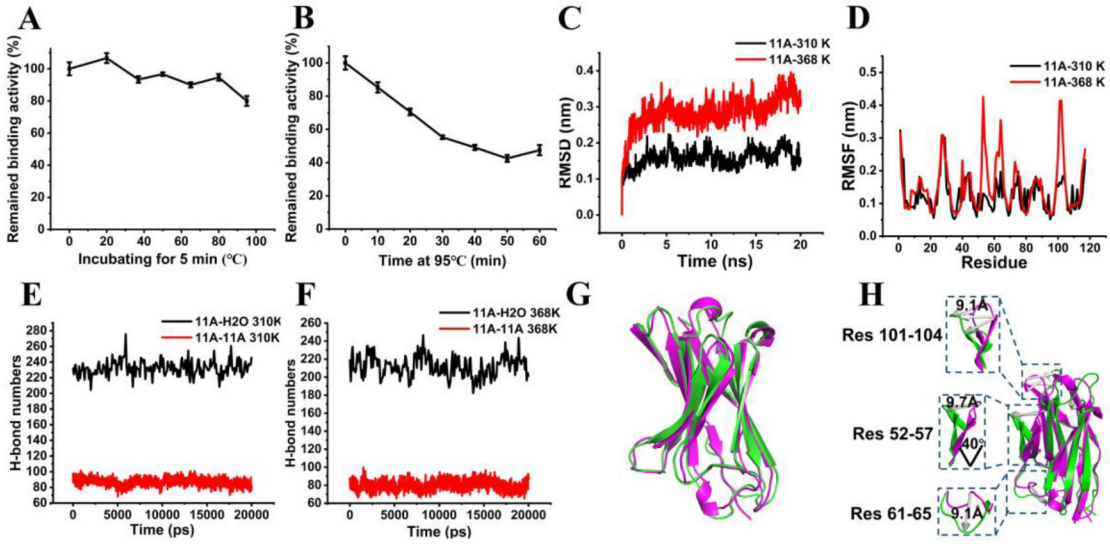

Figure 4. The thermostability of Nb-11A.

(**A**) Nb-11A (1 mg/mL) was incubated for 5 min at 20, 37, 50, 65, 80 and 95°C before being analyzed for binding activity by ic-ELISA. (**B**) Nb-11A (1 mg/mL) was incubated at 95°C from 10 min to 60 min before being analyzed for binding activity by ic-ELISA. (**C and D**) The RMSD values (C) and RMSF values (D) during a 20-ns MD simulation for Nb-11A at 310 K and 368 K. (**E and F**) The change of H-bonds number during a 20-ns MD simulation for Nb-11A at 310 K (E) and 368 K (F). (**G and H**) The structure alignment of Nb-11A in MD equilibrium at 310 K (G) and 368 K (H). Nb-11A are shown in magenta for 0 ns and green respectively for 20 ns.

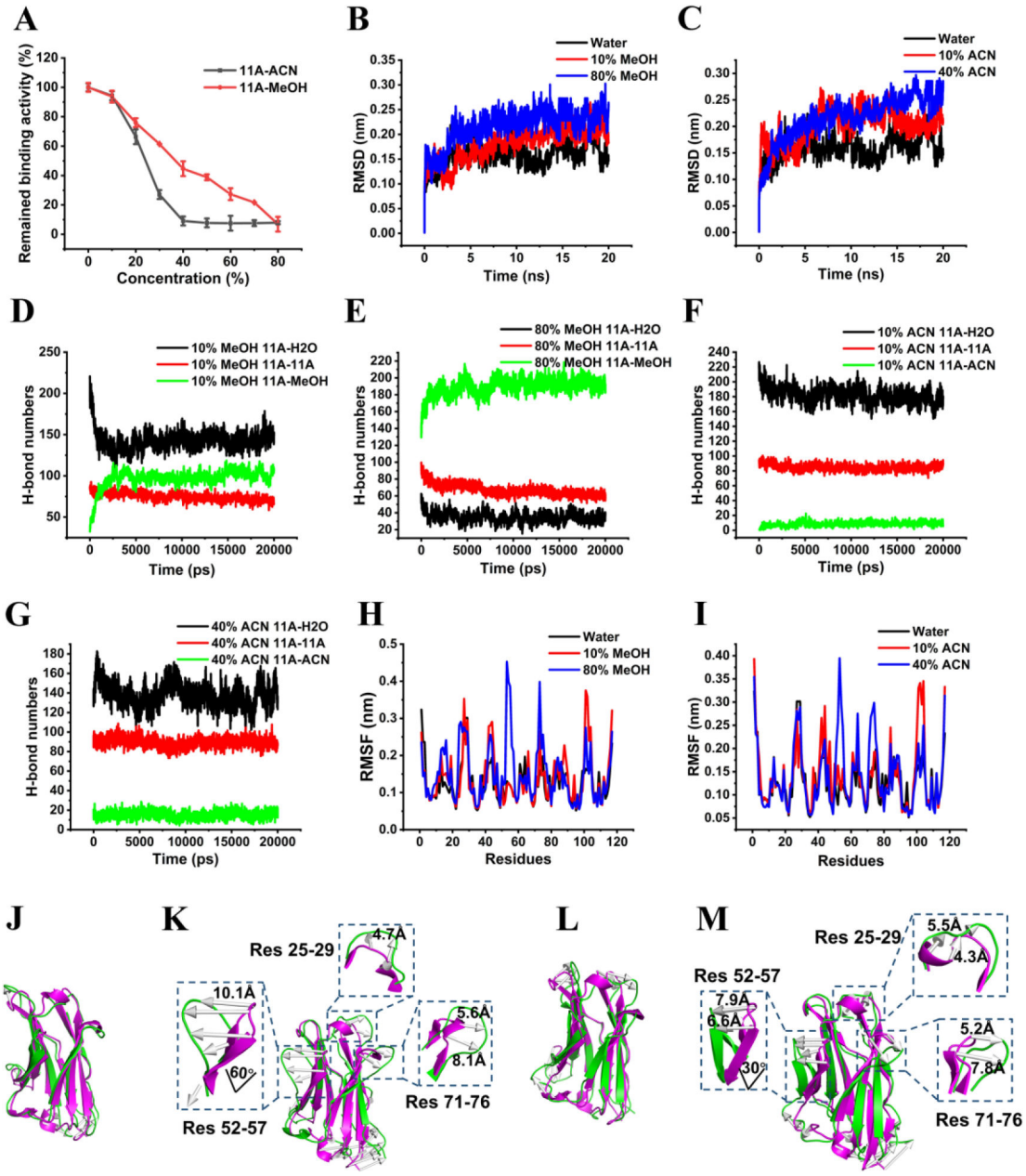

Figure 5. The organic solvents tolerance of Nb-11A.

(**A**) The organic solvent tolerance of Nb-11A. (**B and C**) The RMSD values during a 20-ns MD simulation for Nb-11A in MeOH (B) and ACN (C). (**D to G**) The change of H-bonds number during a 20-ns MD simulation for Nb-11A in 10% MeOH (D), 80% MeOH (E), 10% ACN (F) and 40% ACN (G). (**H to I**) The RMSF values during a 20-ns MD simulation for Nb-11A in MeOH (H) and CAN (I). (**J to M**) The structure alignment of Nb-11A in MD equilibrium in 10% MeOH (J), 80% MeOH (K), 10% ACN (L) and 40% ACN (M). Nb-11A are shown in magenta for 0 ns and green respectively for 20 ns.

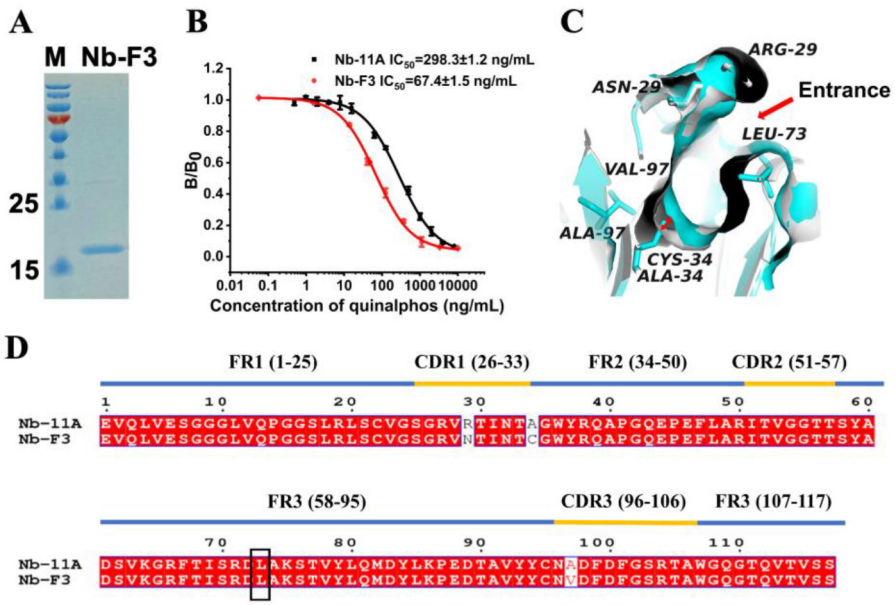

Figure 6. The preparation and identification of Nb-11A mutant Nb-F3.

(**A**) SDS-PAGE analysis of purified Nb-F3. (**B**) The standard curve of ic-ELISA based on Nb-F3. (**C**) The cross-section view of binding pocket of Nb-11A (in gray) and Nb-F3 (in cyan). The key sites are shown in sticks and labeled. The red double-headed arrow indicated the main gap on bottom. (**D**) The sequence alignment of Nb-11A and Nb-F3.

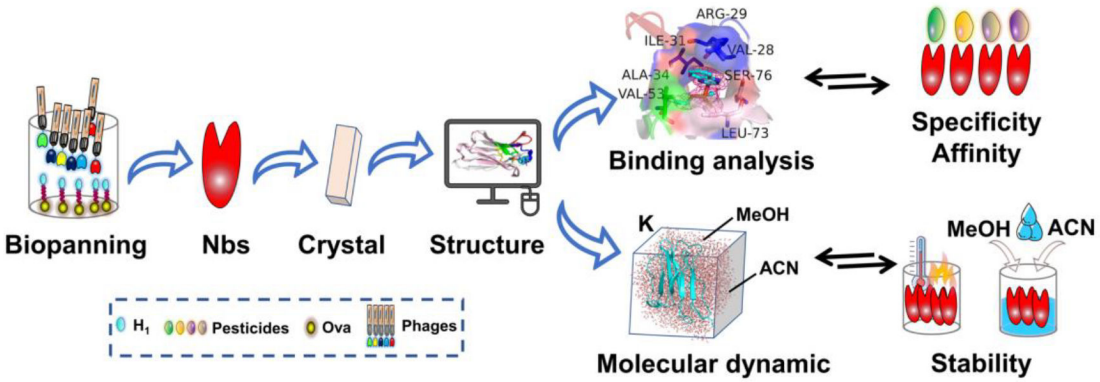

Scheme 1. Workflow of the preparation and structural analysis of the anti-quinalphos nanobody.